Mitochondrial antigen-specific CD8$^+$ T cells drive dopamine neuron neurodegeneration

Moustafa N Elemeery[1,2,3,4,5,6,7], Alex Tchung[2,3,4,7,8], Salix Boulet S[6], Nicolas Giguère[2,3,4,5,7,8], Sarah Mezrag[6,9,10], Jean-Francois Daudelin[4,6], Amandine Even[2,3,4,7,8], Abigail Ralph[4,12], Sriparna Mukherjee [4,8], Claudie Beaulieu[1,2,3,4,7,8], Diana Matheoud[1,11], Jo-Ann Stratton[4,12], Nathalie Labrecque[4,9,10,13]*, Louis-Eric Trudeau[1,2,3,4,7,8]*

*Co-corresponding authors

[1]Department of neurosciences, Faculty of Medicine, Université de Montréal
[2]Neural Signaling and Circuitry research group (SNC)
[3]Center for Interdisciplinary Research on the Brain and Learning (CIRCA)
[4]Aligning Science Across Parkinson's (ASAP) Collaborative Research Network, Chevy Chase, MD, USA, 20815.
[5]Medical Biotechnology Department, Biotechnology Research Institute, National Research Centre, Dokki, Giza, Egypt
[6]Centre de recherche de l'hôpital Maisonneuve-Rosemont (CRHMR)
[7] Courtois Institute for Biomedical Innovation (Ci2B)
[8]Department of pharmacology and physiology, Faculty of Medicine, Université de Montréal
[9]Institut de recherches cliniques de Montréal (IRCM)
[10]Department of microbiology, infectious diseases and immunology, Faculty of Medicine, Université de Montréal
[11]Research Center of the Université de Montréal Hospital (CRCHUM)
[12]Dept. of Neuroscience and Neurology, Montreal Neurological Institute-Hospital, McGill University, Montreal,
[13]Department of medicine, Faculty of Medicine, Université de Montréal

Corresponding authors:

Dr. Louis-Éric Trudeau
Department of pharmacology and physiology
Faculty of Medicine
Université de Montréal
louis-eric.trudeau@umontreal.ca
514-343-5692

Dr. Nathalie Labrecque
Institut de recherches cliniques de Montréal
Department of medicine, Faculty of medicine
Université de Montréal
nathalie.labrecque@umontreal.ca
514-987-550

Running Title: CD8 T cells drive dopamine neuron loss

Summary

The progressive degeneration of dopamine (DA) neurons drives motor symptoms in Parkinson's disease (PD). Whether this neuronal degeneration is due to cell-autonomous dysfunctions in DA neurons or to death signals generated by other cell types is a key problem to address. Recent evidence suggests that loss of function of the protein PINK1, linked to early-onset forms of PD, enhances the presentation of self-derived mitochondrial antigens, which induces the response of autoreactive $CD8^+$ T cells. Whether mitochondrial antigen-specific $CD8^+$ T cells alone are sufficient to induce nigrostriatal dysfunction has not been directly tested. Here we performed adoptive transfer of mitochondrial antigen-specific $CD8^+$ T cells into wild-type or PINK1-deficient mice. We provide evidence for the entry and persistence of such cells in the brain and show that this leads to levodopa-reversible motor dysfunctions and partial degeneration of the nigrostriatal DA system in both genotypes. These findings establish that brain entry of autoreactive $CD8^+$ T cells is sufficient to drive nigrostriatal degeneration and parkinsonian motor deficits, providing the most direct support to date for the hypothesis that an adaptive immune attack plays a key role in PD-like neurodegeneration.

62 **Introduction**

63 The cardinal motor symptoms of Parkinson's disease (PD) are driven in part by the selective and
64 progressive degeneration of dopamine (DA) neurons in the substantia nigra pars compacta (SNc), leading
65 to striatal DA depletion and disruption of basal ganglia circuits controlling movement dynamics. Although
66 DA replacement therapy can transiently restore motor function, no disease-modifying therapies currently
67 exist. Genetic studies in familial forms of PD have implicated defects in fundamental cellular systems,
68 such as in mitochondria, lysosomes and vesicular trafficking, arising from loss-of-function variants in
69 genes such as *Pink1*, *Prkn* (Parkin), *Lrrk2* or *Gba* [1-9]. Such mutations lead to defects across multiple
70 cell types, including neurons, but also immune cells [1, 10]. How these cellular defects translate into the
71 selective neuronal vulnerability seen in PD represents a fundamental unanswered question.

72 Immune cells and inflammatory mechanisms are increasingly considered as playing a role in the
73 initiation or progression of PD. Notably, cytokines such as IL-1β, TNF-α, IFN-γ, IL-6 and IL-8 are
74 elevated in the serum, cerebrospinal fluid and nigrostriatal tissue from PD patients relative to age-matched
75 controls [11-15]. The presence of T cells in the brain of PD subjects has also been reported [13, 16, 17]
76 and T cells recognizing specific antigens like α -synuclein and PINK1 have been detected in the blood of
77 PD patients [18-21]. Interestingly, overexpression of α-synuclein in mice leads to brain entry of $CD4^+$
78 T-cells, neuroinflammation and DA neuron loss in mice and rats [22-25]. Immune mechanisms are also
79 increasingly recognized as triggered by loss-of-function of PINK1 or Parkin, shown to disinhibit
80 mitochondrial antigen presentation (MitAP) on MHC class I molecules in antigen-presenting cells (APCs)
81 [1]. Strikingly, in *Pink1*$^{-/-}$ mice, gastrointestinal infection leads to an increased abundance of mitochondrial
82 antigen-specific $CD8^+$ T cells in the periphery and the loss of striatal DA-terminal markers as well as
83 L-DOPA-reversible motor deficits [26]. These findings support a paradigm shift suggesting that
84 autoimmune mechanisms act as a prime driver of neuronal loss in some forms of PD [10, 27, 28].

85 A critical unanswered question is whether brain entry of autoreactive mitochondrial
86 antigen-specific $CD8^+$ T cells is sufficient to induce DA system dysfunction. To address this possibility,
87 we took advantage of transgenic mice that express a T cell receptor (TCR) specific for a mitochondrial
88 antigen derived from 2-oxoglutarate dehydrogenase (OGDH) [29, 30]. OGDH represents a uniquely
89 relevant autoantigen in the context of PD. OGDH is a highly abundant, matrix-localized mitochondrial
90 protein expressed in all cells including in DA neurons [31]. Importantly, OGDH-derived peptides are
91 selectively presented on MHC class I molecules following mitochondrial stress or in absence of PINK1
92 or Parkin in antigen-presenting cells [1, 26]. This presentation could then induce the response of OGDH-
93 specific $CD8^+$ T cells which may then attack DA neurons upon entry in the central nervous system. We
94 hypothesized that peripheral adoptive transfer of pre-activated mitochondrial antigen specific $CD8^+$ T cells
95 into *Pink1*$^{-/-}$ mice would result in brain infiltration and targeted attack of the DA system. Compatible with
96 this hypothesis, we report that such transfer leads to L-DOPA-reversible motor impairment and robust
97 loss of SNc DA neurons and striatal axonal markers in both WT and *Pink1*$^{-/-}$ mice. Such findings suggest
98 that neuronal loss of PINK1 function in *Pink1*$^{-/-}$ mice may not be a necessary contributor to the induction
99 of neurodegeneration. This work provides a new perspective on immune mechanisms capable of driving
100 PD pathology. Importantly, our observation of $CD8^+$ T-cell-mediated loss of DA neurons also in WT mice
101 raises the possibility that similar mechanisms could also be at play in sporadic forms of PD.

102 **Results**
103
104 **Mitochondrial antigen-specific $CD8^+$ T cells infiltrate the brain and are found in higher numbers in**
105 ***Pink1*$^{-/-}$ mice.**

106 We tested the hypothesis that mitochondrial antigen-specific $CD8^+$ T-cells (thereafter called Mito-T) can
107 induce PD-like pathology and parkinsonism in mice following their adoptive transfer into *Pink1*$^{-/-}$ mice.
108 To do so, we purified $CD8^+$ T cells from 2C TCR transgenic mice, in which $CD8^+$ cells express a TCR

109 specific for the mitochondrial antigen OGDH and adoptively transferred 5 X 10^6 *in vitro* activated $CD8^+$
110 cells by intra-peritoneal (i.p.) injection into WT or *Pink1*$^{-/-}$ mice (**Fig. 1A and Supplementary Fig. 1A**).
111 As a control, WT and *Pink1*$^{-/-}$ mice were adoptively transferred with activated $CD8^+$ T cells (thereafter
112 called OVA-T) from OT-I TCR transgenic mice, expressing a TCR specific for the ovalbumin antigen,
113 not found in mice. Forty-eight hours after adoptive transfer, pertussis toxin (PTx) (20 µg/kg) was
114 administered i.p. to facilitate brain infiltration of the transferred $CD8^+$ T cells, as typically done in rodent
115 multiple sclerosis models. Blood samples were collected on days 7 and 40 after adoptive transfer to assess
116 the persistence and abundance of the transferred cells. The transferred cells were tracked using a
117 monoclonal antibody (1B2) specific for the TCR expressed by the Mito-T $CD8^+$ T cells or with the K^b-
118 OVA tetramer for control OVA-T $CD8^+$ T cells. The gating strategy is described in **Supplementary Fig.**
119 **1B-C**. We successfully detected the transferred Mito-T and OVA-T cells in the blood of the recipient mice
120 at both time points, with a higher frequency of the Mito-T compared to the OVA-T cells (**Fig. 1B-C**).
121 Although the proportion of Mito-T cells in the blood of the transferred mice was not significantly different
122 between *Pink1*$^{-/-}$ and WT mice (**Fig. 1B-C**), the absolute number of such cells detected in the spleen at day
123 40 was higher in the *Pink1*$^{-/-}$ mice compared to WT littermates (**Fig. 1D**). Altogether, these observations
124 indicate that Mito-T cells accumulate more than OVA-T cells in *Pink1*$^{-/-}$ and WT mice, suggesting that
125 such mitochondrial antigen specific $CD8^+$ T cells encounter their antigen in recipient mice. Moreover, as
126 more Mito-T $CD8^+$ T cells were recovered in *Pink1*$^{-/-}$ mice compared to WT recipients, these findings
127 suggest that they may have seen more mitochondrial antigens in the peripheral tissues of *Pink1*$^{-/-}$ mice.

128 We next asked whether the adoptively transferred Mito-T $CD8^+$ cells were infiltrating the brain of the
129 recipient mice. To assess brain infiltration, mice were administered FITC-conjugated anti-CD45 antibody
130 intravenously 3–5 min before tissue collection to label circulating leukocytes but not parenchymal
131 infiltrating cells (**Supplementary Fig. 1B-C**). Flow cytometry revealed the presence in the brain of both

Mito-T and OVA-T cells at both time points, with higher abundance at day 40 (**Fig. 1E-F**) suggesting local antigen recognition and expansion of Mito-T cells. Strikingly, absolute counts of brain-infiltrating Mito-T cells were greater in *Pink1*$^{-/-}$ mice than in WT littermates (**Fig. 1E-F**). Mito-T cell infiltration in the brain was also associated with an increase of recipient T cells (**Supplementary Fig. 1D**). The findings demonstrate that mitochondrial antigen-specific CD8^{+} T-cells infiltrate and persist within the brain for at least 40 days post-transfer, and that enhanced brain accumulation occurs in the absence of functional PINK1.

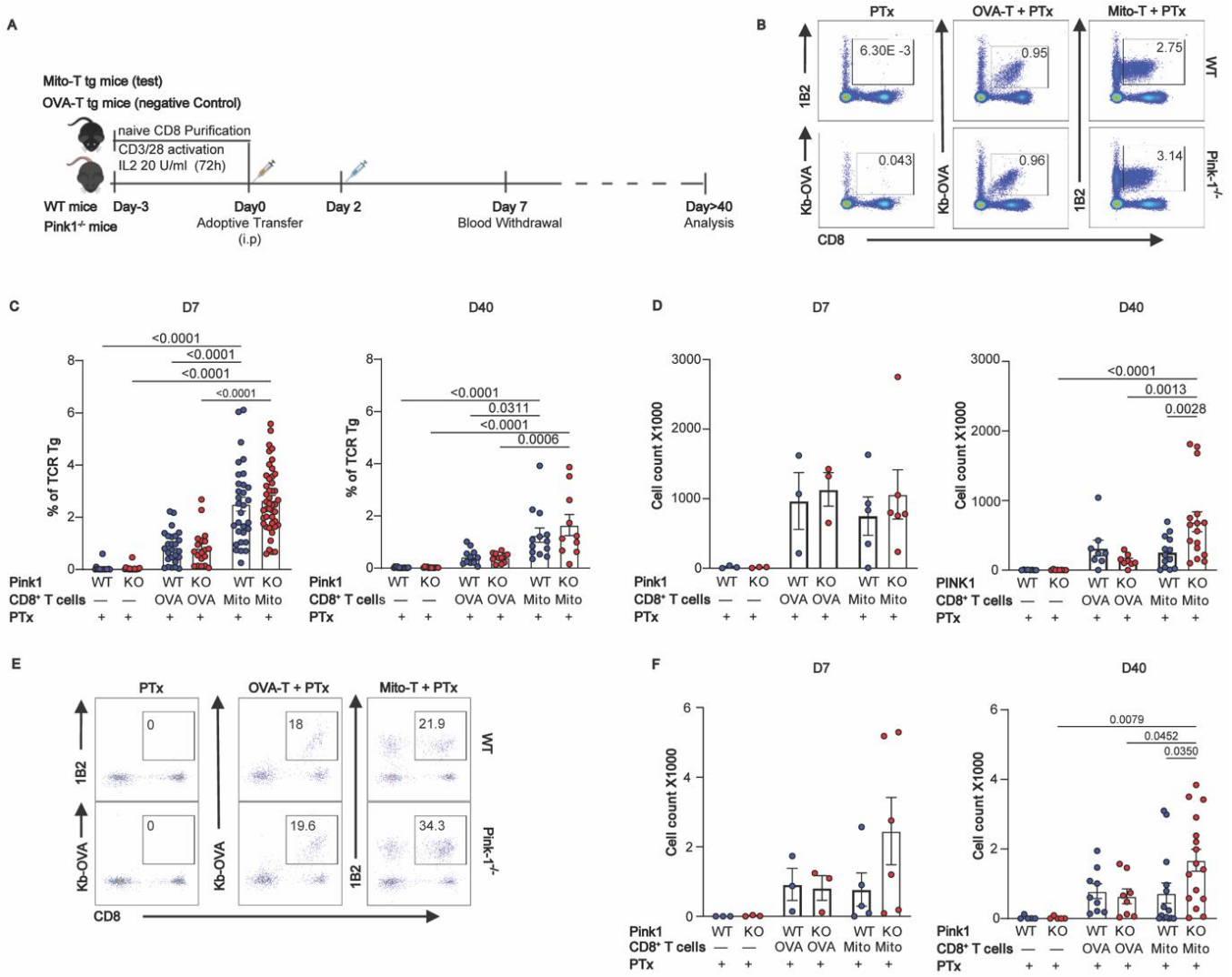

Figure 1: **Adoptively transferred mitochondrial antigen-specific CD8^{+} T cells persist in the circulation and infiltrate the brain in higher amounts in Pink1$^{-/-}$ mice. A.** Schematic diagram outlining the experimental workflow. **B.** Representative flow cytometry profiles for the detection of adoptively transfer TCR transgenic CD8^{+} T cells. Mito-T cells were identified using the

142 anti-TCR clonotype antibody 1B2 ($CD8^+1B2^+$) while OVA-T $CD8^+$ T cells were identified using the K^b-OVA tetramer
143 ($CD8^+K^b$-OVA^+). PTx refers to mice that were not adoptively transferred and only received the Ptx treatment. **C.** Frequency of
144 the adoptively transferred TCR transgenic $CD8^+$ T cells in the blood at day 7 and 40 after the adoptive transfer in WT and
145 $Pink1^{-/-}$ mice. D. Absolute number of adoptively transferred TCR transgenic $CD8^+$ T cells in the spleen of WT and $Pink1^{-/-}$
146 mice. **E.** Representative flow cytometry profiles for the detection of adoptively transfer TCR transgenic $CD8^+$ T cells that have
147 infiltrated into the brain. **F.** Absolute number of adoptively transferred TCR transgenic $CD8^+$ T cells that infiltrated the brain
148 of WT and $Pink1^{-/-}$ mice at 7 days (left) and 40 days (right) after the adoptive transfer. Each dot represents the results obtained
149 from one mouse. Data is representative of a minimum of three independent experiments. p values were determined using two-
150 way ANOVA followed by Tukey's multiple comparisons post-hoc test. Data are presented as mean ± s.e.m. Data from 3
151 independent experiments, male and female mice were pooled.

152

153 **Adoptive transfer of mitochondrial antigen-specific $CD8^+$ T cells induces L-DOPA reversible motor**
154 **impairment in both *Pink1*$^{-/-}$ and WT mice.**

155 Our observation of entry of the adoptively transferred $CD8^+$ T cells in the brain raised the possibility that
156 Mito-T cells recognize their antigen in the brain, leading to DA neuron loss and motor circuit dysfunction.
157 Compatible with this hypothesis, qualitative observations of the animals in their home cage revealed that
158 after a period of 30-40 days following the adoptive transfer, some of the mice showed impaired
159 locomotion. To validate this, we performed more extensive behavioral phenotyping using open field
160 locomotor analysis, grip strength analysis, a rotarod task and the pole test. In the open field, we found
161 reduced movement distance and vertical episodes in the mice transferred with Mito-T cells, but not in the
162 mice transferred with OVA-T cells or only injected with PTx (**Fig. 2A-B**). Similar effects were seen in
163 *Pink1*$^{-/-}$ and WT recipients. Movement time (total ambulation + stereotypy) and average movement
164 velocity were also reduced in the Mito-T condition, while the number of rest episodes did not differ
165 between the groups (**Supplementary Fig. 2**). Time spent in the center of the open field (thigmotaxis),

often used as an indirect index of anxiety, was not altered (**Fig. 2C**). Grip strength was also unaffected (**Fig. 2D**), suggesting preserved muscle force. In the rotarod task, the maximal speed leading to falling off the apparatus and the time to fall was lower in the mice that received Mito-T cells compared to the other groups (**Fig. 2E**), independently of genotype. Finally, in the pole test, the mice with adoptive transfer of Mito-T cells, but not the mice transferred with OVA-T cells or treated only with PTx showed impaired performance, as revealed by a slower time to descend (**Fig. 2F,** left panel), a deficit abolished by pre-treatment with the DA synthesis precursor L-DOPA (**Fig. 2F,** right panel), arguing that the motor impairments observed in the adoptively transferred mice were linked to reduced DA levels. Like for the other behavioral tests, *Pink1*$^{-/-}$ and WT littermates did not differ, suggesting that a similar neurodegenerative process occurred in both genotypes.

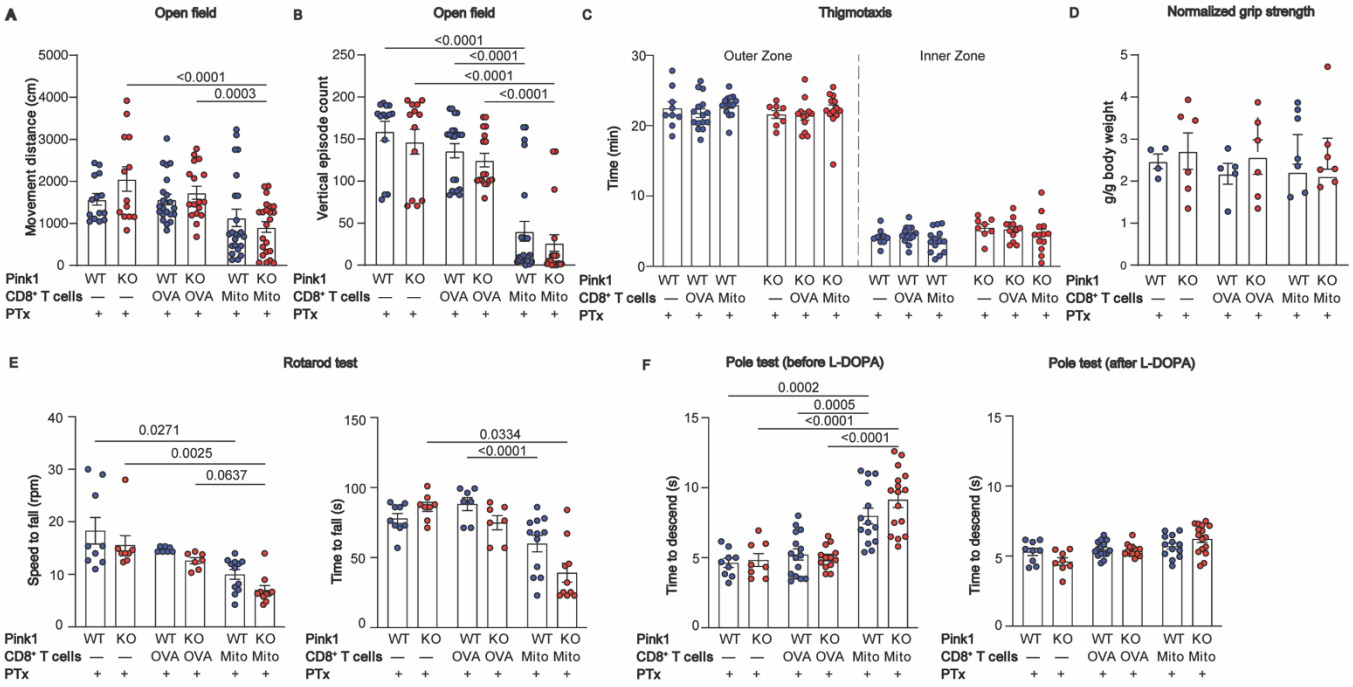

Figure 2: **Adoptive transfer of mitochondrial antigen-specific CD8⁺ T cells leads to L-DOPA reversible motor impairment.** Motor functions were analyzed between days 42 and 56 after the adoptive T cell transfer. **A.** In the open field test, the mice were examined for a period of 30min. The total movement distance travelled by the mice in an open field arena was measured. **B.** Vertical episodes (number of time that the mouse rears). **C.** Time spent in the outer zone vs inner zone of the open field. **D.** Grip strength for the four limbs normalized by mouse body weight. **E.** Rotarod analysis of the maximal speed and time to fall. **F.** Time to descend in the pole test before (left panel) and 15-30 min after i.p. administration of L-DOPA (25mg/kg) and the dopadecarboxylase inhibitor benserazide (6.5 mg/kg) (right panel). Data are representative of four independent experiments for A, B, C, and F and three independent experiments for D and E. p values were determined via two-

way ANOVA followed by Tukey's multiple comparisons test. Data are presented as mean ± s.e.m. The data combines both male and female mice.

Adoptive transfer of mitochondrial antigen–specific CD8$^+$ T cells induces degeneration of nigrostriatal dopamine neurons

The motor dysfunctions observed after adoptive transfer of Mito-T CD8$^+$ T cells suggested impairment of basal ganglia circuitry, a system critically dependent on DA and known to be particularly vulnerable to cellular stress. Since DA neurons can express MHC class I and potentially present antigens to CD8$^+$ T cells [32], we hypothesized that infiltration of Mito-T cells into the brain would directly compromise the nigrostriatal DA system. To test this, we performed immunohistochemical analyses of the striatum from mice 30-40 days post-transfer. In the dorsal striatum, the primary projection target of SNc neurons and the region most severely affected in PD, recipients of Mito-T cells exhibited marked reductions in tyrosine hydroxylase (TH) immunoreactivity. This decrease reached statistical significance in *Pink1*$^{-/-}$ but not in WT mice, which showed more variable effects (**Fig. 3A-B**). No loss was observed in OVA-T cells recipients or in PTx-only controls. Importantly, the density of serotonin neuron axon terminals (SERT immunoreactivity) and the total number of intrinsic striatal neurons (NeuN) remained unchanged across all groups (**Figs. 3A-B**), suggesting that the degenerative process was selective for DA neuron projections. These findings suggest a direct CD8$^+$ T cell attack of DA neurons, impacting the axonal domain, providing an explanation for the impaired behavioral performance of mice that received Mito-T CD8$^+$ T cells.

We next asked whether striatal TH loss reflected selective axon terminal degeneration or was instead a consequence of cell body loss in the ventral midbrain. Unbiased stereological counts of TH$^+$ neurons revealed a significant reduction of DA neuron cell bodies in the SNc in recipients of Mito-T cells compared to OVA-T controls (**Fig. 3C-D**). In contrast, the number of VTA DA neurons was unchanged (**Fig. 3D**). The magnitude of SNc cell body loss was comparable in both *Pink1*$^{-/-}$ and WT mice (**Fig. 3D**), and no differences were observed in the number of non-DA neurons in either region (**Fig. 3E**).

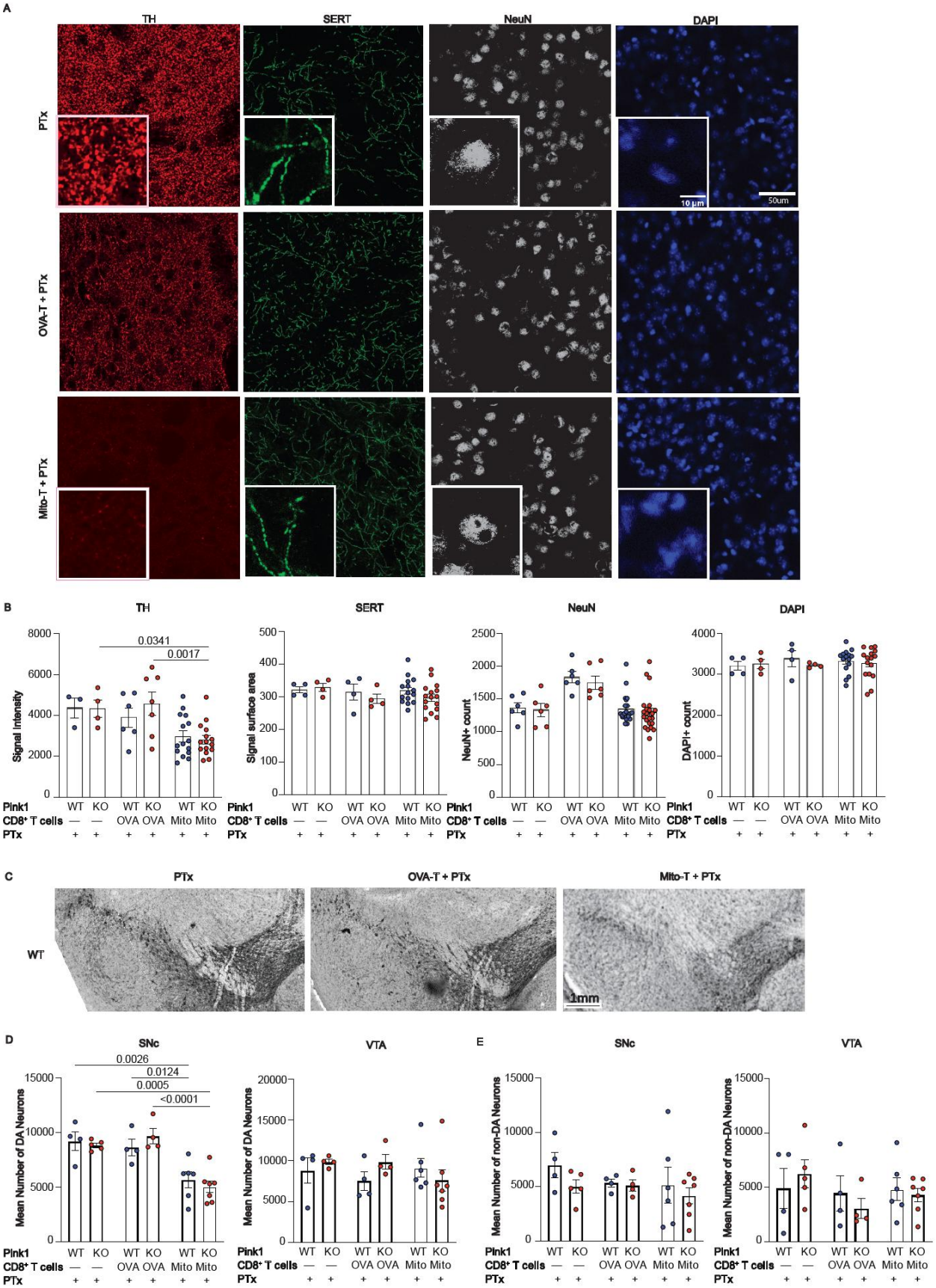
A
TH
SERT
NeuN
DAPI
PTx
OVA-T + PTx
Mito-T + PTx
10 µm
50um
B
TH
SERT
NeuN
DAPI
Signal intensity
Signal surface area
NeuN+ count
DAPI+ count
0.0341
0.0017
Pink1 WT KO WT KO WT KO
CD8+ T cells — — OVA OVA Mito Mito
PTx + + + + + +
C
PTx
OVA-T + PTx
Mito-T + PTx
WT
1mm
D
SNc
VTA
Mean Number of DA Neurons
0.0026
0.0124
0.0005
<0.0001
E
SNc
VTA
Mean Number of non-DA Neurons

210

211 ***Figure 3:*** **Adoptive transfer of mitochondrial antigen–specific CD8$^+$ T cells cause selective dopaminergic denervation.**
212 **A.** Immunofluorescence staining of the dorsal striatum of Pink1$^{-/-}$ and WT mice shows dopaminergic neuronal markers tyrosine
213 hydroxylase (TH, red). Serotonergic terminals were visualized using the serotonin transporter (SERT, green), neuronal nuclei
214 with NeuN (grey), and total nuclei with DAPI (blue). **B.** Quantification of axon terminal marker signal intensities revealed a
215 selective reduction of TH but not SERT, NeuN or DAPI, consistent with selective dopaminergic denervation in Pink1$^{-/-}$ mice
216 after adoptive transfer of mitochondrial antigen–specific CD8$^+$ T cells. NeuN and DAPI are represented as absolute cell counts
217 per unit area. **C.** Representative images of the DAB staining used for stereological counting of TH$^+$ DA neurons in the ventral
218 midbrain. **D,E.** Stereological counting of TH$^+$ (DA neurons) and non-DA neurons in the ventral tegmental area (VTA) and
219 substantia nigra pars compacta (SNc). Data pooled from three independent experiments. Brains were collected 42–56 days
220 post-transfer. Statistical significance was determined by two-way ANOVA followed by Tukey's multiple comparisons test.
221 Data are shown as mean ± s.e.m.
222

223 Microglia and astrocytes are increasingly considered to be involved in mediating neuroinflammatory and
224 neurodegenerative processes in PD. For example, the number of microglia labelled with Iba1 is increased
225 in many mouse PD models [33, 34]. We therefore next sought to determine whether the persistent presence
226 of T cells in the mice after adoptive transfer was accompanied by sustained activation of resident glial
227 populations. We examined brain sections at a sub-chronic phase, 30 days after adoptive transfer of Mito-
228 T or OVA-T cells. Quantification of Iba1$^+$ microglial immunostaining [35] in dorsal striatum revealed no
229 significant differences in mean fluorescence intensity between Mito-T, OVA-T or control mice
230 (**Supplementary figure 3A**). To confirm these histological findings, we performed Western blot analysis
231 of dissected striata and SNc tissue blocks. The protein levels of Iba1 and of the astrocytic marker GFAP
232 were not significantly altered in Mito-T or OVA-T mice compared with controls (**Supplementary figure**
233 **3B**).While these observations do not exclude the presence of functional changes in these cells, these results
234 indicate that at this point, adoptive transfer of activated mitochondrial antigen specific CD8$^+$ T cells does
235 not induce broad or sustained upregulation of microglial or astrocytic markers in the striatum or SNc.
236 Collectively, these results demonstrate that adoptive transfer of mitochondrial antigen–specific CD8$^+$ T
237 cells can trigger selective degeneration of nigrostriatal DA neurons, resulting in both loss of striatal
238 terminals and degeneration of SNc cell bodies. Moreover, once T cells infiltrate the CNS, they elicit
239 comparable SNc neuronal soma loss in both WT and *Pink1*-deficient mice.
240

241 **Adoptively transferred CD8$^+$ T cells acquire a memory-like phenotype**

242 The persistence of the adoptively transferred CD8$^+$ T cells within the CNS for up to 40 days prompted us
243 to examine whether they have undergone differentiation into memory T cells, providing a potential
244 explanation for the lag time between the initial entry of the adoptively transferred cells in the brain and
245 the appearance of motor dysfunctions and neuronal loss. Flow cytometric profiling of brain-infiltrating
246 CD8$^+$ T cells at day 40 post-transfer revealed that both Mito-T and control OVA-T cells acquired a
247 memory phenotype. These cells exhibited high expression of CD44, CD127, and Ly6C, together with low
248 expression of the exhaustion marker PD-1, consistent with long-lived, functionally competent memory T
249 cells rather than terminally exhausted cells (**Fig. 4A–C**). Both Mito-T and OVA-T cells isolated from the
250 brain expressed CXCR3 and CXCR6 providing an explanation for CNS tropism (**Fig. 4A**). The different
251 subsets of memory, effector, resident or central T cells were all detected in the brain **(Fig. 4C).** These
252 findings suggest Mito-T cells persist as memory CD8$^+$ T cells, and even establish residency, in a phenotype
253 poised for antigen recognition and effector function within the CNS. Notably, although Mito-T and OVA-
254 T cells displayed largely overlapping phenotypic profiles, the total number of recovered brain-infiltrating
255 cells differed between the two populations, indicating that antigen specificity influenced their
256 accumulation or persistence within the CNS rather than their differentiation state.

257 A key complementary question is whether these brain-infiltrating CD8$^+$ T cells are functional, i.e.
258 producing cytokines and cytotoxic molecules. To tackle this question, Mito-T and OVA-T cells isolated
259 from the brain 30 days after adoptive transfer were examined for the production of effector molecules
260 (IFN-γ, TNF-α, IL-17 and granzyme B). As very few cells were recovered, the sorted cells (CD45.2$^+$)
261 were mixed with congenic B6SJL splenocytes (CD45.1$^+$) (**Fig. 4D**) before *in vitro* stimulation with PMA
262 and ionomycin for 5h to assess their effector functions. The brain-infiltrating memory CD8$^+$ T cells
263 produced high levels of IFN-γ, granzyme B, and TNF-α, whereas IL-17A production was almost non-

264 detectable (**Fig. 4E-F**), consistent with a classical type 1 cytotoxic (Tc1) effector profile. The production
265 of effector molecules was also observed in OVA-T cells as expected for cells with a memory phenotype.
266 Altogether, our results demonstrate that the adoptive transfer of mitochondrial antigen specific $CD8^+$ T
267 cells leads to their accumulation as functional memory T cells in the brain. Their robust cytotoxic effector
268 function suggests that they are endowed with the capacity to provoke neuronal injury, providing an
269 explanation for the degeneration of DA neurons observed in the mice after adoptive transfer of Mito-T
270 $CD8^+$ T cells.
271

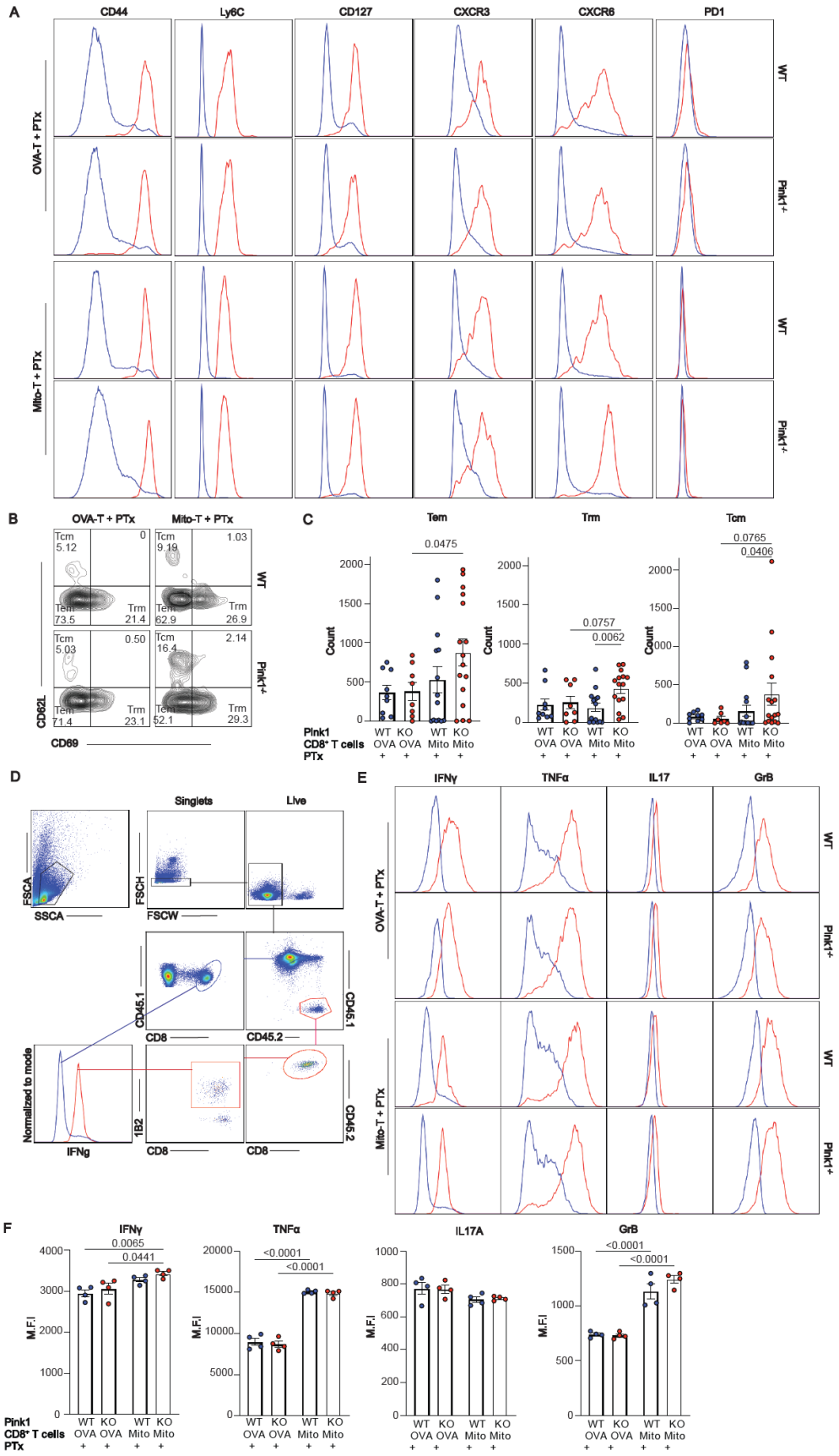
A
CD44
Ly6C
CD127
CXCR3
CXCR6
PD1
OVA-T + PTx
Mito-T + PTx
WT
Pink1-/-
B
OVA-T + PTx
Mito-T + PTx
Tcm
Tem
Trm
CD62L
CD69
C
Tem
Trm
Tcm
Count
Pink1
CD8+ T cells
PTx
WT
KO
OVA
Mito
D
Singlets
Live
FSCA
SSCA
FSCH
FSCW
CD45.1
CD45.2
CD8
Normalized to mode
IFNg
1B2
E
IFNγ
TNFα
IL17
GrB
F
IFNγ
TNFα
IL17A
GrB
M.F.I

272

273 *Figure 4:* **Brain-infiltrating CD8$^+$ T cells acquire a memory phenotype and retain effector function following adoptive**
274 **transfer. A.** Representative flow cytometry plots showing expression of memory- and homing-associated markers (CD44,
275 Ly6C, CXCR3, CXCR6, CD127, and PD-1) on brain-infiltrating CD8$^+$ T cells isolated 40 days after adoptive transfer of OVA-
276 T or Mito-T CD8$^+$ T cells into WT or Pink1$^{-/-}$ recipient mice treated with PTx (red) vs rest of CD45$^+$cells in the brain (blue).
277 **B.** Representative flow cytometry profile of CD69 and CD62L expression on brain-infiltrating CD8$^+$ T cells, allowing
278 discrimination of tissue-resident memory (Trm; CD69$^+$CD62L$^-$), effector memory (Tem; CD69$^-$CD62L$^-$), and central memory
279 (Tcm; CD69$^-$CD62L$^+$) subsets. **C.** Quantification of the different memory CD8$^+$ T cell subsets among OVA-T and Mito-T
280 populations recovered from the brain of WT and Pink1$^{-/-}$ mice. **D.** Flow cytometry gating strategy for assessment of effector
281 function in brain-infiltrating CD8$^+$ T cells. CD45.2$^+$ donor-derived T cells isolated from the brain 30 days post-transfer were
282 mixed with congenic CD45.1$^+$ B6SJL splenocytes and stimulated ex vivo with PMA and ionomycin prior to intracellular
283 cytokine staining. **E.** Representative flow cytometry plots showing intracellular expression of IFN-γ, TNF-α, GrB, and IL-17A
284 in OVA-T and Mito-T CD8$^+$ T cells (red) vs B6SJL CD8$^+$ cells (blue) following stimulation. **F.** Quantification of mean
285 fluorescence intensity (MFI) for IFN-γ, TNF-α, granzyme B, and IL-17A in donor-derived TCR$^+$ CD8$^+$ T cells. Data is
286 representative of two independent experiments. p values were determined using two-way ANOVA followed by Tukey's
287 multiple comparisons test. Data are presented as mean ± s.e.m. Data from male and female mice were pooled.
288

289 ## Discussion

290 The origin of neuronal degeneration in PD is an unsolved mystery. A large body of work has examined
291 and documented the possibility that the loss of DA neurons results from cell-autonomous dysfunctions in
292 these neurons. This includes the hypothesis that pathological aggregation of the protein α-synuclein leads
293 to cellular dysfunctions in DA neurons and the activation of apoptosis [36-38]. Or that aggregation of α-
294 synuclein leads to reduced levels of monomeric forms of this protein, with loss of function mechanisms
295 leading to neuronal demise [39, 40]. It has also been hypothesized that environmental exposure to some
296 pesticides leads to the loss of DA neurons by blocking the mitochondrial complex 1 in these cells [41].
297 Partial support for this hypothesis comes from the observation that conditional deletion of mitochondrial
298 complex 1 gene products in DA neurons leads to age-dependent gradual impairment of the DA system in
299 mice [42-44].
300

301 An equally plausible but less examined alternate or complementary hypothesis is that the loss of SNc DA
302 neurons results from dysfunctions in other cell types including glial cells in the brain or peripheral immune
303 cells that gain access to the brain. The work described in the present manuscript adds strong support for
304 such non-cell autonomous mechanisms by showing that brain entry of autoreactive mitochondrial-

305 targeting $CD8^+$ T cells is sufficient to cause the loss of DA neurons and to induce motor dysfunctions, a
306 phenotype suggestive of PD pathology. In accordance with this hypothesis, a growing series of studies
307 focusing on gene products linked to familial, genetic forms of PD, suggest that multiple PD-related
308 proteins including Parkin, PINK1 and LRRK2 act as regulators of innate and adaptive immune responses
309 in antigen presenting cells (APCs) and that loss of function of some of these proteins can amplify immune
310 responses [1, 10, 18-20, 27, 28, 45-47]. Recent work revealed that in inflammatory conditions, PINK1
311 and Parkin restrict the presentation on MHC class I molecules of antigens derived from proteins present
312 in the mitochondrial matrix (MitAP) [1]. This led to the hypothesis that a loss of function of PINK1 or
313 Parkin leads to increased presentation of mitochondrial antigens and to the activation of autoreactive $CD8^+$
314 T cells [1]. In keeping with this hypothesis, follow-up work revealed that MitAP can be activated
315 following gut infection with Gram-negative bacteria in *Pink1*$^{-/-}$ mice, a process associated with the
316 activation and expansion of mitochondrial antigen-specific $CD8^+$ T cells and the concomitant
317 development of motor impairments reversible by L-DOPA [26]. Although thought-provoking, a direct
318 role for $CD8^+$ T cells in causing neuronal loss and the emergence of motor impairments was not clearly
319 established in this previous work.
320
321 The present study provides direct evidence that mitochondrial antigen-specific $CD8^+$ T cells alone are
322 sufficient to trigger DA neuron loss and L-DOPA-reversible motor symptoms. Beyond supporting the
323 hypothesis that MitAP and $CD8^+$ T cells are possible initiators of PD-like pathology, our work delineates
324 a clear periphery-to-CNS immune axis where primed autoreactive $CD8^+$ T cells enter the brain, establish
325 a tissue-resident memory phenotype and induce neurodegeneration. This positions mitochondrial
326 autoimmunity as a mechanistic bridge between systemic immune dysregulation and selective neuron loss.
327

328 Although the adoptive transfer of pre-activated antigen-specific $CD8^+$ T cells represents a reductionist
329 experimental approach, this strategy was deliberately designed to isolate and test a single unresolved
330 causal question: whether autoreactive mitochondrial-specific $CD8^+$ T cells are sufficient to induce
331 selective DA neuron degeneration once they gain access to the brain. By removing confounding variables
332 such as infection, α-synuclein overexpression, or generalized inflammation, this model reveals the
333 intrinsic neurodegenerative potential of mitochondrial antigen-specific $CD8^+$ T cells.
334
335 A surprising finding in the present work is that neurodegeneration and motor impairments developed in
336 both *Pink1*$^{-/-}$ and WT mice following mitochondrial-targeted T cell adoptive transfer. Although further
337 work will be required to clarify this, a possibility is that since PINK1 inhibits the presentation of
338 mitochondrial antigens by APCs, one of the main roles of this protein in the context of PD is to prevent
339 the initiation of the disease process by restricting the priming of naive $CD8^+$ T cells in the periphery [48].
340 Accordingly, introducing preactivated cytotoxic T cells by adoptive transfer bypasses the protective
341 function of PINK1 and directly engages a pathophysiological process in both WT and KO mice, as long
342 as some level of MitAP occurs in DA neurons or local glial cells, allowing the autoreactive $CD8^+$ T cells
343 to engage with brain cells. This scenario implies that loss of function of PINK1 in DA neurons may
344 perhaps not be required to engage neuropathological mechanisms in PD once cytotoxic T cells are
345 generated in the periphery. Our work thus provides a different perspective on how PINK1 loss of function
346 could lead to dysfunction and loss of DA neurons. PINK1 was first shown to be involved in the clearance
347 of damaged mitochondria by mitophagy [49-53]. Such observations were taken by some to imply that loss
348 of PINK1 function in DA neurons would lead to the accumulation of damaged mitochondria in these
349 neurons, eventually promoting their death. However, mitophagy still proceeds in the absence of PINK1
350 [54-57] and there is presently very limited evidence that dysfunctional mitochondria indeed accumulate

351 in PINK1 or Parkin KO DA neurons [58]. Although we did not directly evaluate the functions of neuronal
352 PINK1 in the present study, our results are more compatible with the hypothesis that loss of function of
353 PINK1 engages autoimmune mechanisms in the periphery at early stages of the disease process. Our
354 finding of loss of DA neurons even in WT mice raises the thought-provoking hypothesis that the T-cell-
355 mediated neuronal death mechanism identified in the present model could occur not only in individuals
356 carrying mutations in PINK1, but also in sporadic forms of PD. One can hypothesize that age-related
357 decreases in the levels of PINK1 or Parkin [59] in APCs could engage a sequence of events similar to that
358 induced by loss of function mutations.
359
360 The specific cellular and molecular mechanisms by which $CD8^+$ T cells kill DA neurons in the present
361 model remains to be determined. Based on previous work suggesting that DA neurons have the capacity
362 to express MHC class I molecules on their surface [32], one possibility is that in these mice, following
363 entry in the brain of Mito-T cells, DA neurons present mitochondrial antigens leading to their direct
364 recognition and attack by cytotoxic $CD8^+$ T cells. However, more work is needed to characterize the extent
365 and dynamics of MHC class I expression by DA neurons in both *Pink1*$^{-/-}$ and WT mice. Our finding of an
366 equivalent attack of DA neurons by activated Mito-T $CD8^+$ T cells in the two genotypes suggests that a
367 minimally sufficient level of antigen presentation may happen in both genotypes, although not necessarily
368 at the same levels. Further work will be required to clarify this and to examine the alternate possibility
369 that MitAP occurs principally in glial cells, leading to the production of neurotoxic signals by these cells
370 or to reduced production of neurotrophic signals. A growing literature suggests similar mechanisms
371 implicating $CD8^+$ T cells and glial cells in Alzheimer's disease [49, 60-62].
372

373 Our findings further demonstrate that brain-infiltrating antigen-specific $CD8^+$ T cells retain robust effector
374 capacity, as evidenced by their ability to produce IFN-γ, TNF-α, and granzyme B upon *ex vivo* stimulation.
375 This effector profile indicates that infiltrating $CD8^+$ T cells are not functionally exhausted or inert but
376 instead remain poised to mediate inflammatory and cytotoxic responses within the CNS. The presence of
377 granzyme B together with pro-inflammatory cytokines supports a model in which $CD8^+$ T cells may
378 contribute to neuronal injury through both direct cytotoxic mechanisms and indirect amplification of
379 neuroinflammation.
380
381 Taken together, our observations provide unprecedented support for a key role of mitochondrial antigen-
382 specific $CD8^+$ T cells in DA system perturbations and associated parkinsonism in a mouse model of early-
383 onset PD. This work could be instrumental for the development of better animal models of PD and for the
384 identification of new immune-based therapeutic approaches to treat PD patients.
385

386 **Acknowledgements**

387 We would like to thank Drs. Michel Desjardins, Samantha Gruenheid, Heidi McBride and Janelle Drouin-
388 Ouellet for their critical feedback during the development of this project. We also thank Dr. Numa
389 Dancause for providing access to their stereological counting microscope system. We thank Frédéric
390 Duval and Marie-Josée Aubin for cell sorting and the animal care technicians for mice husbandry. The
391 present study was funded by the joint efforts of the Michael J. Fox Foundation for Parkinson's Research
392 (MJFF) and the Aligning Science Across Parkinson's (ASAP) initiative. MJFF administers the grant
393 ASAP 000525 on behalf of ASAP and itself. The Trudeau lab also received support from the Canadian
394 Institutes of Health Research (CIHR) (grant 165928) and from the Krembil foundation. M. N. E. received
395 a graduate student award from the mission sector of the ministry of higher education, Egypt.

Declaration of Interests:

The authors declare that they have no conflicts of interest.

References

1. Matheoud, D., et al., *Parkinson's disease-related proteins PINK1 and Parkin repress mitochondrial antigen presentation.* Cell, 2016. **166**(2): p. 314-327.
2. Drouin-Ouellet, J., et al., *Age-related pathological impairments in directly reprogrammed dopaminergic neurons derived from patients with idiopathic Parkinson's disease.* Stem Cell Reports, 2022. **17**(10): p. 2203-2219.
3. Drouin-Ouellet, J., *Mitochondrial complex I deficiency and Parkinson disease.* Nat Rev Neurosci, 2023. **24**(4): p. 193.
4. Fava, V.M., et al., *Pleiotropic effects for Parkin and LRRK2 in leprosy type-1 reactions and Parkinson's disease.* Proc Natl Acad Sci U S A, 2019. **116**(31): p. 15616-15624.
5. de Leseleuc, L., et al., *PARK2 mediates interleukin 6 and monocyte chemoattractant protein 1 production by human macrophages.* PLoS Negl Trop Dis, 2013. **7**(1): p. e2015.
6. Kim, K.S., et al., *Regulation of myeloid cell phagocytosis by LRRK2 via WAVE2 complex stabilization is altered in Parkinson's disease.* Proc Natl Acad Sci U S A, 2018. **115**(22): p. E5164-E5173.
7. Taylor, M. and D.R. Alessi, *Advances in elucidating the function of leucine-rich repeat protein kinase-2 in normal cells and Parkinson's disease.* Curr Opin Cell Biol, 2020. **63**: p. 102-113.
8. Al-Azzawi, Z.A.M., S. Arfaie, and Z. Gan-Or, *GBA1 and The Immune System: A Potential Role in Parkinson's Disease?* J Parkinsons Dis, 2022. **12**(s1): p. S53-S64.
9. Wallings, R.L., et al., *ASO-mediated knockdown or kinase inhibition of G2019S-Lrrk2 modulates lysosomal tubule-associated antigen presentation in macrophages.* Mol Ther Nucleic Acids, 2023. **34**: p. 102064.
10. Fahmy, A.M., et al., *Mitochondrial antigen presentation: a mechanism linking Parkinson's disease to autoimmunity.* Curr Opin Immunol, 2019. **58**: p. 31-37.
11. Koziorowski, D., et al., *Inflammatory cytokines and NT-proCNP in Parkinson's disease patients.* Cytokine, 2012. **60**(3): p. 762-766.
12. Brockmann, K., et al., *Inflammatory profile discriminates clinical subtypes in LRRK2-associated Parkinson's disease.* Eur J Neurol, 2017. **24**(2): p. 427-e6.
13. Kouli, A., et al., *Neuroinflammation and protein pathology in Parkinson's disease dementia.* Acta Neuropathol Commun, 2020. **8**(1): p. 211.
14. Williams-Gray, C.H., et al., *Serum immune markers and disease progression in an incident Parkinson's disease cohort (ICICLE-PD).* Mov Disord, 2016. **31**(7): p. 995-1003.
15. Wijeyekoon, R.S., et al., *Cerebrospinal Fluid Cytokines and Neurodegeneration-Associated Proteins in Parkinson's Disease.* Mov Disord, 2020. **35**(6): p. 1062-1066.
16. Brochard, V., et al., *scher, J. Callebert, J. Launay, C. Duyckaerts, RA Flavell, EC Hirsch and S. Hunot.* The Journal of Clinical Investigation, 2009. **119**: p. 182-192.
17. Ma, M., et al., *The spatial landscape of glial pathology and T cell response in Parkinson's disease substantia nigra.* Nat Commun, 2025. **16**(1): p. 7146.
18. Sulzer, D., et al., *T cells from patients with Parkinson's disease recognize alpha-synuclein peptides.* Nature, 2017. **546**(7660): p. 656-661.
19. Singhania, A., et al., *The TCR repertoire of alpha-synuclein-specific T cells in Parkinson's disease is surprisingly diverse.* Sci Rep, 2021. **11**(1): p. 302.
20. Lindestam Arlehamn, C.S., et al., *alpha-Synuclein-specific T cell reactivity is associated with preclinical and early Parkinson's disease.* Nat Commun, 2020. **11**(1): p. 1875.

21. Johansson, E., et al., *T cell responses towards PINK1 and alpha-synuclein are elevated in prodromal Parkinson's disease.* NPJ Parkinsons Dis, 2025. **11**(1): p. 137.
22. Schonhoff, A.M., et al., *Border-associated macrophages mediate the neuroinflammatory response in an alpha-synuclein model of Parkinson disease.* Nat Commun, 2023. **14**(1): p. 3754.
23. Williams, G.P., et al., *CD4 T cells mediate brain inflammation and neurodegeneration in a mouse model of Parkinson's disease.* Brain, 2021. **144**(7): p. 2047-2059.
24. Tiberi, M., et al., *Systemic inflammation triggers long-lasting neuroinflammation and accelerates neurodegeneration in a rat model of Parkinson's disease overexpressing human alpha-synuclein.* 2024.
25. Tavira, A., et al., *Inhibition of T cell infiltration and soluble TNF signaling is neuroprotective in the alpha-synuclein overexpressing mouse model of Parkinson's disease.* NPJ Parkinsons Dis, 2025. **11**(1): p. 315.
26. Matheoud, D., et al., *Intestinal infection triggers Parkinson's disease-like symptoms in Pink1(-/-) mice.* Nature, 2019. **571**(7766): p. 565-569.
27. Hobson, B.D. and D. Sulzer, *Neuronal Presentation of Antigen and Its Possible Role in Parkinson's Disease.* J Parkinsons Dis, 2022. **12**(s1): p. S137-S147.
28. Garretti, F., et al., *T cells, alpha-synuclein and Parkinson disease.* Handb Clin Neurol, 2022. **184**: p. 439-455.
29. Sha, W.C., et al., *Selective expression of an antigen receptor on CD8-bearing T lymphocytes in transgenic mice.* Nature, 1988. **335**(6187): p. 271-274.
30. Udaka, K., et al., *Self-MHC-restricted peptides recognized by an alloreactive T lymphocyte clone.* Journal of immunology (Baltimore, Md.: 1950), 1996. **157**(2): p. 670-678.
31. Schmidt, S., et al., *A reversible state of hypometabolism in a human cellular model of sporadic Parkinson's disease.* Nat Commun, 2023. **14**(1): p. 7674.
32. Cebrian, C., et al., *MHC-I expression renders catecholaminergic neurons susceptible to T-cell-mediated degeneration.* Nat Commun, 2014. **5**: p. 3633.
33. Oda, W., et al., *Inhibition of repulsive guidance molecule-a protects dopaminergic neurons in a mouse model of Parkinson's disease.* Cell Death Dis, 2021. **12**(2): p. 181.
34. Verma, D.K., et al., *Alpha-Synuclein Preformed Fibrils Induce Cellular Senescence in Parkinson's Disease Models.* Cells, 2021. **10**(7).
35. Thi Lai, T., et al., *Microglial inhibition alleviates alpha-synuclein propagation and neurodegeneration in Parkinson's disease mouse model.* NPJ Parkinsons Dis, 2024. **10**(1): p. 32.
36. Yan, M., et al., *alpha-Synuclein-mediated mitochondrial translocation of cofilin-1 leads to oxidative stress and cell apoptosis in PD.* Front Neurosci, 2024. **18**: p. 1420507.
37. Patterson, J.R., et al., *Time course and magnitude of alpha-synuclein inclusion formation and nigrostriatal degeneration in the rat model of synucleinopathy triggered by intrastriatal alpha-synuclein preformed fibrils.* Neurobiol Dis, 2019. **130**: p. 104525.
38. Paumier, K.L., et al., *Intrastriatal injection of pre-formed mouse alpha-synuclein fibrils into rats triggers alpha-synuclein pathology and bilateral nigrostriatal degeneration.* Neurobiol Dis, 2015. **82**: p. 185-199.
39. Benskey, M.J., et al., *Silencing Alpha Synuclein in Mature Nigral Neurons Results in Rapid Neuroinflammation and Subsequent Toxicity.* Front Mol Neurosci, 2018. **11**: p. 36.
40. Espay, A.J., et al., *Alpha-synuclein in Parkinson's disease: Embracing debate, exercising skepticism.* Parkinsonism Relat Disord, 2025. **136**: p. 107874.
41. Betarbet, R., et al., *Chronic systemic pesticide exposure reproduces features of Parkinson's disease.* Nat Neurosci, 2000. **3**(12): p. 1301-6.

42. Gonzalez-Rodriguez, P., et al., *Disruption of mitochondrial complex I induces progressive parkinsonism.* Nature, 2021. **599**(7886): p. 650-656.
43. Sterky, F.H., et al., *Altered dopamine metabolism and increased vulnerability to MPTP in mice with partial deficiency of mitochondrial complex I in dopamine neurons.* Hum Mol Genet, 2012. **21**(5): p. 1078-89.
44. Ekstrand, M.I., et al., *Progressive parkinsonism in mice with respiratory-chain-deficient dopamine neurons.* Proc Natl Acad Sci U S A, 2007. **104**(4): p. 1325-30.
45. Williams, G.P., et al., *Unaltered T cell responses to common antigens in individuals with Parkinson's disease.* J Neurol Sci, 2023. **444**: p. 120510.
46. Nguyen, M., et al., *Parkinson's genes orchestrate pyroptosis through selective trafficking of mtDNA to leaky lysosomes.* bioRxiv, 2023: p. 2023.09. 11.557213.
47. Fahmy, A.M., et al., *LRRK2 regulates the activation of the unfolded protein response and antigen presentation in macrophages during inflammation.* bioRxiv, 2023: p. 2023.06. 14.545012.
48. Recinto, S.J., et al., *PINK1 deficiency rewires early immune responses in a mouse model of Parkinson's disease triggered by intestinal infection.* NPJ Parkinsons Dis, 2025. **11**(1): p. 133.
49. Laurent, C., et al., *Hippocampal T cell infiltration promotes neuroinflammation and cognitive decline in a mouse model of tauopathy.* Brain, 2017. **140**(1): p. 184-200.
50. Narendra, D.P., et al., *PINK1 is selectively stabilized on impaired mitochondria to activate Parkin.* PLoS Biol, 2010. **8**(1): p. e1000298.
51. Geisler, S., et al., *PINK1/Parkin-mediated mitophagy is dependent on VDAC1 and p62/SQSTM1.* Nat Cell Biol, 2010. **12**(2): p. 119-31.
52. Kawajiri, S., et al., *PINK1 is recruited to mitochondria with parkin and associates with LC3 in mitophagy.* FEBS Lett, 2010. **584**(6): p. 1073-9.
53. Matsuda, N., et al., *PINK1 stabilized by mitochondrial depolarization recruits Parkin to damaged mitochondria and activates latent Parkin for mitophagy.* J Cell Biol, 2010. **189**(2): p. 211-21.
54. Dagda, R.K., et al., *Loss of PINK1 function promotes mitophagy through effects on oxidative stress and mitochondrial fission.* J Biol Chem, 2009. **284**(20): p. 13843-13855.
55. McWilliams, T.G., et al., *Basal Mitophagy Occurs Independently of PINK1 in Mouse Tissues of High Metabolic Demand.* Cell Metab, 2018. **27**(2): p. 439-449 e5.
56. Oshima, Y., et al., *Parkin-independent mitophagy via Drp1-mediated outer membrane severing and inner membrane ubiquitination.* J Cell Biol, 2021. **220**(6).
57. Miyazaki, N., et al., *PINK1-dependent and Parkin-independent mitophagy is involved in reprogramming of glycometabolism in pancreatic cancer cells.* Biochem Biophys Res Commun, 2022. **625**: p. 167-173.
58. Giguere, N., et al., *Comparative analysis of Parkinson's disease-associated genes in mice reveals altered survival and bioenergetics of Parkin-deficient dopamine neurons.* J Biol Chem, 2018. **293**(25): p. 9580-9593.
59. Tokarew, J.M., et al., *Age-associated insolubility of parkin in human midbrain is linked to redox balance and sequestration of reactive dopamine metabolites.* Acta Neuropathol, 2021. **141**(5): p. 725-754.
60. Chen, X., et al., *Microglia-mediated T cell infiltration drives neurodegeneration in tauopathy.* Nature, 2023. **615**(7953): p. 668-677.
61. Jorfi, M., et al., *Infiltrating CD8(+) T cells exacerbate Alzheimer's disease pathology in a 3D human neuroimmune axis model.* Nat Neurosci, 2023. **26**(9): p. 1489-1504.
62. Su, W., et al., *CXCR6 orchestrates brain CD8(+) T cell residency and limits mouse Alzheimer's disease pathology.* Nat Immunol, 2023. **24**(10): p. 1735-1747.

537 63. Hogquist, K.A., et al., *T cell receptor antagonist peptides induce positive selection.* Cell, 1994.
538 **76**(1): p. 17-27.
539 64. HJ, G., *The new stereological tools: disector, fractionator, nucleator and point sampled intercepts*
540 *and their use in pathological research and diagnosis.* Apmis, 1988. **96**: p. 857-881.

541
542
543 **Materials and methods**

544

545 **Mice.** The 2C TCR-transgenic mice (RRID:MGI:3621454) express a TCR recognizing an OGDH
546 mitochondrial peptide presented by MHC class I K^b [29, 30], The OT-I TCR-transgenic mice
547 (RRID:IMSR_JAX:003831) express a TCR specific for the $OVA^{257–264}$ peptide presented by MHC class
548 I K^b [63]. Male and female *Pink1*$^{-/-}$ mice (Jackson Laboratory, Strain #017946, RRID:
549 IMSR_JAX:017946) and WT littermate controls were bred and housed under specific pathogen-free
550 conditions. All mice were maintained in accordance with the Canadian Council on Animal Care
551 guidelines, under protocols approved by the animal ethics committee (Comité de déontologie de
552 l'expérimentation animale, CDEA) of the Université de Montréal and of the Research Center of the
553 Maisonneuve-Rosemont Hospital.

554

555 **T cell purification and activation.** Naïve $CD8^+$ T cells were isolated from the spleen of 2C and OT-I
556 TCR transgenic mice using a Easysep™ mouse naïve $CD8^+$ T-cell isolation kit (STEMCELL,
557 Technologies, cat# 19858). Purified naïve $CD8^+$ T cells were then activated using plate-bound anti-CD3
558 antibody (clone 14-2C11, Bio X Cell, cat# BE0001-1, RRID: AB1107634) and a soluble anti-CD28
559 antibody (clone 37.51, Bio X Cell, cat# BE0015-1, RRID: AB1107624). Briefly, 24-well plates were
560 coated with 1 µg/ml of anti-CD3 antibody in sterile PBS and incubated for 2h at 37°C, 5% CO2. 2 x 10^6
561 naïve $CD8^+$ T cells were seeded per well, and anti-CD28 antibody was added to a final concentration of 5
562 µg/ml. After 24h, recombinant mouse IL-2 (50 IU/mL, PeproTech, cat# 212-12) was added, and cells were

563 maintained for 72h at 37 °C and 5 % CO_2. Activation was confirmed by flow cytometry analysis of
564 up-regulation of CD44, CD25 and CD69 and down-regulation of CD62L.
565
566 **Adoptive transfer of TCR transgenic T cells**. *Pink1*$^{-/-}$ mice and their WT littermate controls were
567 injected intraperitoneally (i.p) with 5 X 10^6 *in vitro*-activated mitochondrial OGDH peptide specific CD8
568 T cells (Mito-T) derived from 2C TCR mice or OVA-257-264 peptide specific $CD8^+$ T cells (OVA-T)
569 derived from OT-I TCR mice, as a negative control. Cells were resuspended in 200 µl of sterile PBS
570 immediately prior to injection. Control groups included mice receiving PBS but no T-cells. Forty-eight
571 hours after adoptive transfer, all experimental animals received pertussis toxin (PTx; 20 µg/kg i.p.,
572 Cayman Chemical, cat# 23221) to facilitate T-cell entry into the central nervous system by transiently
573 increasing blood–brain barrier permeability.
574
575 **FACS analysis.** Blood samples (200 µl) were collected from the jugular vein into 100ul PBS containing
576 2mM EDTA at both early (day 7) and late (day 40) time points following the adoptive transfer. Spleens
577 were harvested at day 7 from a subset of mice and from all the mice at the experimental endpoint. Red
578 blood cells were lysed in 0.86% ammonium chloride (NH_4CL) solution for 5 min at room temperature,
579 followed by washing in PBS. Cell viability was assessed with Zombie NIR™ fixable viability dye (1:1000
580 in PBS; BioLegend, cat# 423105, RRID: AB_2565394) for 20 min at room temperature in the dark.
581 Samples were then blocked with anti-CD16/CD32 (Fc Block; clone 2.4G2, BD Biosciences, cat# 553142,
582 RRID: AB_394657) for 20 min at room temperature prior to surface staining. Surface marker staining was
583 performed for 20 min at 4 °C in FACS buffer (Dulbecco's PBS without phenol red supplemented with
584 3 % heat-inactivated fetal bovine serum, 10 mM HEPES, and 0.1 % sodium azide).

585 To identify OVA-T cells, samples were stained with H-2K^b- OVA-257-264 peptide tetramer (NIH
586 Tetramer core facility) and staining was performed at 37°C for 15 min at 37 °C before the antibody
587 cocktail. Data acquisition was performed on a BD LSRFortessa™ X-20 flow cytometer (BD Biosciences,
588 RRID:SCR_023638), and analysis was performed using FlowJo™ (BD Biosciences,
589 RRID:SCR_008520). All antibodies (with clone, fluorochrome, manufacturer, catalog number, and
590 RRID) are listed in **Supplementary Table 1**.
591
592 **Intracellular staining and effector function analysis.** To assess effector function of brain-infiltrating
593 CD8$^+$ T cells, intracellular cytokine and granzyme B stainings were performed following short-term *ex*
594 *vivo* stimulation. Brain-infiltrating leukocytes were isolated as described below followed by cell sorting
595 of CD8$^+$CD45.2$^+$ cells. Due to the low yield of infiltrating T cells, sorted CD8$^+$CD45.2$^+$ T cells were
596 mixed with congenic CD45.1$^+$ B6.SJL splenocytes as carrier cells prior to stimulation. Cell suspensions
597 were stimulated for 5h at 37 °C and 5 % CO_2 with phorbol 12-myristate 13-acetate (PMA, 50 ng/ml;
598 Sigma-Aldrich) and ionomycin (1 µg/ml; Sigma-Aldrich) in complete RPMI-1640 medium. Brefeldin A
599 (5 µg/ml; BioLegend) and monensin (2 µM; BioLegend) were added for the duration of the stimulation
600 to block cytokine secretion. Following stimulation, cells were washed and stained with Zombie NIR™
601 fixable viability dye, followed by Fc receptor blocking (anti-CD16/32) and surface staining for CD45.1,
602 CD45.2, CD8α, CD44 and TCR (1B2 or K^b-OVA). Cells were then fixed and permeabilized using the
603 Cyto-Fix/Cyto-Perm™ kit (BD Biosciences) according to the manufacturer's instructions. Intracellular
604 staining was performed for interferon-γ (IFN-γ), tumor necrosis factor-α (TNF-α), interleukin-17A (IL-
605 17A), and granzyme B. Samples were acquired on a BD LSRFortessa™ X-20 flow cytometer, and data
606 were analyzed using FlowJo™ software. Effector molecule production was quantified within viable
607 CD45.2$^+$CD8$^+$1B2$^+$ (for Mito-T) or CD45.2$^+$CD8$^+$K^b-OVA$^+$ (for OVA-T) T cells after exclusion of

608 CD45.1^{+} carrier splenocytes. Unstimulated controls were included to define background staining and
609 gating thresholds.
610
611 **Isolation of brain infiltrating lymphocytes.** To distinguish infiltrated brain T cells from those still in
612 circulation, mice were injected intravenously (i.v) with anti-CD45-FITC antibody (clone 30-F11, BD
613 Biosciences, cat# 553080, RRID: AB_394609) 3–5 min before sacrifice for brain harvest. T cells shielded
614 from this brief intravascular staining were considered to be localized within the brain parenchyma and
615 were detected as CD45-FITC negative during flow cytometry analysis. Brains were dissected and minced
616 longitudinally into ≥8 fragments using a sterile scalpel, then enzymatically digested in RPMI
617 supplemented with 0.01 mg/ml DNase I (Roche, cat# 11284932001, RRID:SCR_019337) and 0.5 mg/ml
618 collagenase D (Roche, cat# 11088858001, RRID:AB_2827424) for 40 min at 37 °C using the
619 gentleMACS™ Octo Dissociator (Miltenyi Biotec, cat# 130-096-427). Cell suspensions were passed
620 through a 70 µm cell strainer (Corning, cat# 352350) to remove debris. For lymphocyte enrichment, the
621 digested tissue was centrifuged at 1500 rpm for 10 min, resuspended in 3 ml of 37% Percoll (Cytiva,
622 cat# 17-0891-01) diluted in RPMI-1640, overlaid onto 3 ml of 70% Percoll, and centrifuged at 2000 rpm
623 for 20 min at 25 °C without brake. The brain-infiltrating leukocyte fraction was collected from the
624 interphase for downstream flow cytometry analysis.
625
626 **Immunohistochemistry.** *Pink1*$^{-/-}$ and WT littermate mice that had received adoptive transfer of CD8^{+}
627 T-cells or control treatments were deeply anaesthetized with pentobarbital (70 µg/g body weight, i.p.;
628 Wisent Bioproducts, cat# 450-166-XL) and perfused intracardially with 50 ml ice-cold PBS (0.01 M)
629 followed by 50 ml ice-cold 4 % paraformaldehyde (PFA).

630 Brains were collected, post-fixed for 24h at 4°C in 4% PFA, then cryoprotected for 48h in 30% sucrose
631 prepared in phosphate buffer (5.382g/l sodium phosphate monobasic, 8.662g/l sodium phosphate dibasic
632 anhydrous; Sigma-Aldrich). Serial coronal free-floating sections (40µm) were obtained using a Leica
633 CM1950 cryostat and stored in antifreeze solution (1.57g/l sodium phosphate monobasic anhydrous,
634 5.45g/L sodium phosphate dibasic anhydrous, 300ml ethylene glycol, 300ml glycerol, distilled water to
635 volume) at −20 °C. Sections were permeabilized in 0.1% Triton™ X-100 (Sigma-Aldrich, cat# T8787)
636 and blocked in 10 % BSA (Sigma-Aldrich, cat# A2153), containing 0.02 % sodium azide, 0.3 % Triton
637 X-100, and 5% goat serum for 1h at room temperature. Overnight incubation (4 °C) was performed with
638 primary antibodies: rabbit anti-TH (1:2000, AB152; Millipore, cat# AB152, RRID:AB_390204), rabbit
639 anti-Sert (1:2000; Millipore, cat# PC177L-100UL, RRID:AB_10697452) or mouse anti-NeuN (1:1000;
640 Abcam, cat# ab134014, RRID:AB_2313589). Nuclei were counterstained with DAPI (1:2000;
641 Sigma-Aldrich, cat# D9542).
642
643 For the quantification of TH immunoreactivity in the striatum, three brain sections from each mouse were
644 acquired from bregma 1.1, 0.14 and -0.94 and images from regions of interest including the whole striatum
645 were obtained from both hemispheres and acquired using a 20X, 0.8 NA, plan apochromat objective on a
646 Zeiss Axioscan 7 slide scanner (Zeiss Canada). Scans from whole striata were acquired for TH under
647 identical exposure and illumination settings across all experimental groups to ensure quantitative
648 comparability. TH terminal density was estimated by quantifying mean signal intensity across analyzed
649 striatal fields. In separate experiments aimed at quantifying SERT, NeuN, DAPI or Iba1, images were
650 acquired on a Nikon AX-R automated point-scanning confocal microscope (Nikon Instruments,
651 RRID:SCR_023799) at 2048x2048 px resolution, Nyquist sampling, galvanometer scanning mode, with
652 1x averaging and 0.8ms dwell time, using a Plan Apo λ 40×/0.95 OFN25 DIC N2 objective lens (0.6 NA,

653 Nikon Canada). For these quantifications, images were acquired from dorsal striatum fields, defined as
654 the area superior to the anterior commissure and inferior to the corpus callosum. For each striata, 2-4
655 random fields per hemisphere were imaged. Quantification was performed in FIJI/ImageJ (NIH,
656 RRID:SCR_002285) by applying a uniform background-subtracted threshold to all analyzed images.
657 SERT+ terminal density was calculated as mean signal area across eight fields per dorsal striatum, with 5
658 sections/mouse. The number of NeuN-positive and DAPI-positive cells was quantified from the same
659 image sets.
660
661 **Stereological analysis.** Coronal brain sections were rinsed in 0.01 M PBS (1×) for 10 min and immersed
662 in 0.01 M PBS containing 0.9 % H_2O_2 for 10 min to quench endogenous peroxidase activity. Sections were
663 rinsed 3× in PBS (10 min each) and incubated for 48h at 4 °C with rabbit anti TH antibody (1:1000;
664 Millipore, cat# AB152, RRID:AB_390204) diluted in 0.01 M PBS containing 0.3 % Triton X 100 (Sigma
665 Aldrich, cat# T8787) and 50 mg/ml bovine serum albumin (BSA; Sigma Aldrich, cat# A2153). Coronal
666 brain sections were rinsed in 0.01 M PBS (1X) for 10 min before immersed in 0.01 M PBS containing
667 0.9% H_2O_2 for 10 min to quench endogenous peroxidase activity. Sections were rinsed three times in 0.01
668 M PBS (10 min each) after which they were incubated for 48h at 4 °C with rabbit anti-TH antibody
669 (1:1000; Millipore, cat# AB152, RRID:AB_390204) diluted in 0.01 M PBS containing 0.3 % Triton X
670 100 (Sigma Aldrich, cat# T8787) and 50 mg/ml bovine serum albumin (BSA; Sigma Aldrich,
671 cat# A2153). Sections were rinsed 3× in PBS and incubated for 12h at 4 °C with biotin conjugated
672 AffiniPure IgG (1:200; Jackson ImmunoResearch, cat# RON1231, RRID: AB_2337238). After washing
673 3× in PBS, sections were incubated for 3h at room temperature in streptavidin HRP conjugate (1:200;
674 Cytiva/GE Healthcare, cat# RPN1231) diluted in 0.3 % Triton X 100/PBS. Visualization was performed
675 using a 3,3′-diaminobenzidine tetrahydrochloride DAB)–glucose oxidase reaction (Sigma-Aldrich,

676 cat# D8001) for 5 min. Sections were mounted onto charged microscope slides (Thermo Scientific,
677 cat# J1800AMNZ) in 0.1 M acetate buffer, counterstained with cresyl violet (Sigma Aldrich, cat# HT901),
678 dehydrated in graded ethanol, cleared in xylene, and finally cover slipped with Permount™ (Fisher
679 Scientific. Cat # SP15-100). Unbiased stereological counts of TH^+ neurons in the SNc and VTA were
680 performed using the optical fractionator method [64] using Stereo Investigator v6 (MBF Bioscience,
681 RRID:SCR_002526) at 100× magnification, with a 60 × 60 μm^2 counting frame, a 10 µm optical dissector,
682 and two 1 µm guard zones. Sections were sampled every sixth slice, with counting sites placed at 100 µm
683 intervals after a random start. A minimum of 6 sections per mouse containing the SNc was set as an
684 inclusion criterion.
685
686 **Behavioral tests.** All behavioral experiments were conducted during the dark (active) phase of the
687 light/dark cycle, with mice maintained on a 12h light/12 h dark schedule (lights off 22:00–10:00). The
688 experimenter was blinded to both genotype and the treatment group throughout all testing procedures. To
689 minimize handling stress, mice were habituated to the experimenter for not less than 5 min per mouse on
690 3-5 consecutive days prior to testing. Mice were group housed (2-4 per cage) and tested 42-52 days post
691 adoptive transfer. On testing days, mice were moved to the behavioral testing room and allowed to
692 acclimate for 60 min before the start of assay.
693
694 **Basal locomotor activity.** Basal locomotor activity was assessed using open field automated activity
695 chambers (Superflex, Omnitech Electronics, Columbus, OH, USA) to quantify horizontal activity and
696 vertical rearing episode. Mice were placed individually in clear acrylic activity arenas (41 × 41 cm)
697 equipped with arrays of infrared photocell beams to detect movement. Horizontal and vertical activity was

698 recorded continuously over 30 min by counting beam interruptions. Data were analyzed using Fusion
699 software v5.3 (Omnitech Electronics, RRID:SCR_022276).
700
701 **Grip strength test.** Muscular strength was measured with a grip strength meter (model BIO GS3, Bioseb,
702 Vitrolles, France). Each mouse was weighed immediately prior to testing to allow normalization of
703 strength data to body weight. For each trial, the mouse was gently allowed to grasp the metal grid with all
704 four paws, and the peak force (g force) required to dislodge the animal was recorded. Three consecutive
705 trials were performed per mouse, and the average peak force was calculated for analysis. Results are
706 presented as gram force normalized to body weight (g/g).
707
708 **Pole test.** The pole test apparatus consisted of a 60 cm high metal rod (10 mm diameter) wrapped in
709 adhesive tape to improve grip, mounted securely in a test cage. For each trial, mice were placed head up
710 at the top of the pole. Two parameters were recorded: (1) time to orient downward and (2) total time to
711 descend until the forepaws reached the cage floor. Mice were first tested drug naïve and then re-tested 15–
712 30 min after i.p. administration of either benserazide hydrochloride (6.5 mg/kg; Sigma Aldrich,
713 cat# B7283) combined with L DOPA (25 mg/kg; Sigma Aldrich, cat# D1507) or an equal volume of sterile
714 saline. A maximum cut off time of 180 s was imposed; mice exceeding this limit were scored as failures
715 and returned to their home cage. Such mice were re-tested after a rest period.
716
717 **Western Blot Assay** Total protein lysates from brain tissue were prepared using Pierce™ RIPA Lysis
718 Buffer (Thermo Scientific, cat# 89900) supplemented with complete™ EDTA free protease inhibitor
719 (1 tablet/50 mL; Roche, cat# 11873580001) and PhosSTOP™ phosphatase inhibitor (Roche,
720 cat# 04906837001). Protein concentrations were determined with the Pierce™ BCA Protein Assay Kit

721 (Thermo Scientific, cat# 23227), and 20 µg total protein per sample was loaded for SDS PAGE. Proteins
722 were separated on Mini PROTEAN® TGX™ precast gels (Bio Rad, cat# 456 1094) at 200 V for 40 min
723 and transferred to Immobilon PVDF membranes (MilliporeSigma, cat# IPVH00010) at 100 V for 90 min.
724 Membranes were blocked in PBST (PBS + 0.4 % Tween 20) containing 5 % non-fat dry milk for 30 min
725 at room temperature, then incubated overnight at 4 °C with primary antibodies diluted in PBS containing
726 1 % bovine serum albumin (BSA; Sigma Aldrich, cat# A2153). Following 3 × 15 min washes in PBST,
727 membranes were incubated with the appropriate HRP conjugated secondary antibodies (Jackson
728 ImmunoResearch, various) in PBST + 5 % milk for not less than 30 min at room temperature, washed
729 again 3 × 15min in PBST, and developed using Clarity™ Western ECL Substrate (Bio Rad, cat# 170
730 5061). Chemiluminescence was visualized with a ChemiDoc™ MP Imaging System (Bio Rad,
731 RRID:SCR_019037).
732
733
734 **Statistical Analysis.** Statistical analyses were performed using GraphPad Prism v10.0 (GraphPad
735 Software, RRID:SCR_002798). The Mann–Whitney U test was used for 2 group comparisons; one way
736 or two-way ANOVAs with Tukey's post hoc test were used to compare 3 or more groups, as appropriate.
737 Significance was set at $p < 0.05$. Data are presented as mean ± SEM unless otherwise specified.

Data and materials availability:

All key data is included in the manuscript. Access to original raw images is available on request from the corresponding authors.